

doi.org/10.1002/minf.202100028

In silico Studies on the Interaction between Mpro and PLpro From SARS-CoV-2 and Ebselen, its Metabolites and Derivatives

Pablo Andrei Nogara,^[a] Folorunsho Bright Omege,^[a] Gustavo Roni Bolzan,^[a] Cássia Pereira Delgado,^[a] Michael Aschner,^[b] Laura Orian,^[c] and João Batista Teixeira Rocha^{*[a]}

Abstract: The COVID-19 pandemic caused by the SARS-CoV-2 has mobilized scientific attention in search of a treatment. The cysteine-proteases, main protease (Mpro) and papain-like protease (PLpro) are important targets for antiviral drugs. In this work, we simulate the interactions between the Mpro and PLpro with Ebselen, its metabolites and derivatives with the aim of finding molecules that can potentially inhibit these enzymes. The docking data demonstrate that there are two main interactions between the thiol (–SH) group of Cys (from the protease active sites) and the electrophilic centers of the organoselenium molecules, i.e. the interaction with the carbonyl group (O=C⁺–SH) and the interaction with the Se moiety (Se⁺–SH). Both inter-

actions may lead to an adduct formation and enzyme inhibition. Density Functional Theory (DFT) calculations with Ebselen indicate that the energetics of the thiol nucleophilic attack is more favorable on Se than on the carbonyl group, which is in accordance with experimental data (Jin et al. *Nature*, 2020, 582, 289–293). Therefore, organoselenium molecules should be further explored as inhibitors of the SARS-CoV-2 proteases. Furthermore, we suggest that some metabolites of Ebselen (e.g. Ebselen diselenide and methyl-ebselenoxide) and derivatives ethaselen and ebsulfur should be tested *in vitro* as inhibitors of virus replication and its proteases.

Keywords: COVID-19 · protease · organoselenium · docking · DFT

1 Introduction

The COVID-19 (Corona Virus Disease 2019) global respiratory pandemic is caused by the severe acute respiratory syndrome coronavirus 2 (SARS-CoV-2). COVID-19 has already afflicted millions people, globally near 128 millions have been infected and more than 2.8 million have died (data from <https://coronavirus.jhu.edu/map.html>, last access: 31 Mar 2021). The majority of infected people (~80%) are asymptomatic or presents mild symptoms, similar to the common flu.^[1–3] However, severe cases, which require hospitalization, are characterized by fever and dry cough, which can evolve to pneumonia, severe inflammation (cytokine storm), thrombosis, kidney failure, and central nervous system symptoms (encephalitis, seizures) and death.^[3–7]

Of particular therapeutic significance, the cysteine-proteases from coronavirus (MERS-CoV, SARS-CoV, and SARS-CoV-2) have been considered potential targets for the development of antiviral drugs.^[8,9,18,19,10–17] The viral proteases process the large polyprotein (pp1a and pp1ab) forming critical nonstructural proteins (nsp) for the replication and packaging of new viruses inside the host cells.^[5,20,21] The main protease (Mpro, also called 3C-like protease - 3CLpro) and the papain-like protease (PLpro) have one cysteine (Cys) residue in their active site. The reactive cysteinyl residue in Mpro has been implicated as


the target for potential pharmacological agents, such as Ebselen (EbSe, 2-phenyl-1,2-benzoselenazol-3-one, or PZ-51).^[9,22–24]

EbSe has been found to inhibit the SARS-CoV-2 Mpro and PLpro *in vitro* with an IC₅₀ ranging from 0.7 to 2.4 μM, apparently via the formation of an EbSe adduct with the active site cysteine of the enzymes.^[9,22,25] Importantly, EbSe is a safe and approved drug for use in humans, and although it has been tested in several clinical trials (treatment of brain ischemia, cardiovascular complications of diabetes, noise-induced hearing loss), its therapeutic effi-

[a] P. A. Nogara, F. B. Omege, G. R. Bolzan, C. P. Delgado, J. B. Teixeira Rocha
Departamento de Bioquímica e Biologia Molecular, Universidade Federal de Santa Maria (UFSM), Santa Maria, 97105-900, RS, Brazil
E-mail: jbtrocha@yahoo.com.br

[b] M. Aschner
Department of Molecular Pharmacology, Albert Einstein College of Medicine, 1300 Morris Park Avenue, Bronx, NY 10461, USA

[c] L. Orian
Dipartimento di Scienze Chimiche, Università degli Studi di Padova, Via Marzolo 1 35131 Padova, Italy

 Supporting information for this article is available on the WWW under <https://doi.org/10.1002/minf.202100028>

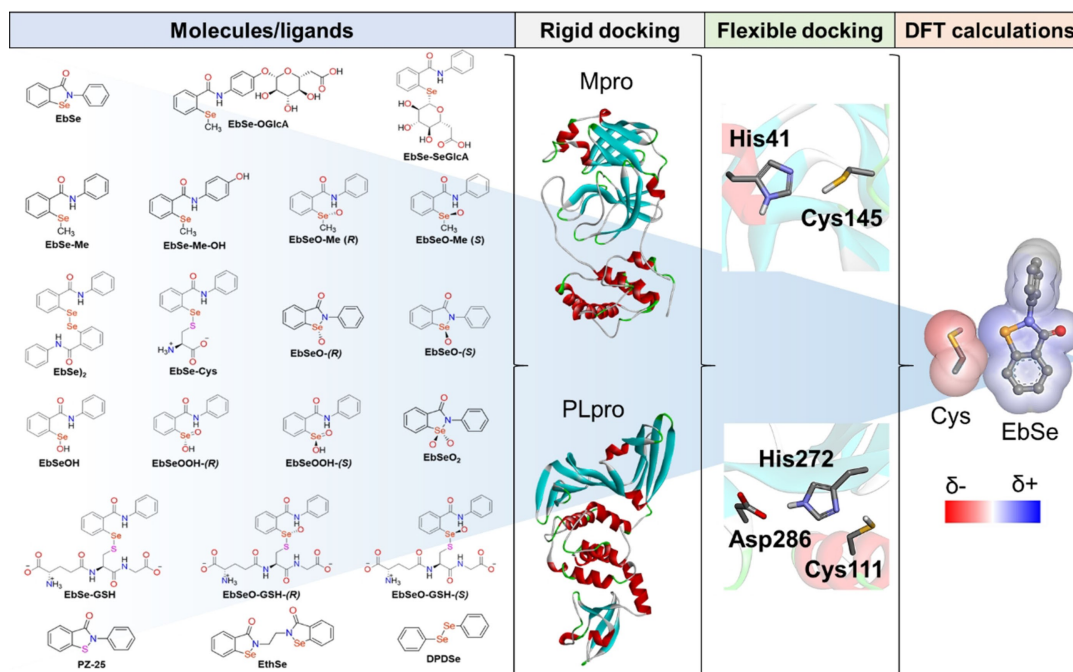


Figure 1. Ebselen, its metabolites, and derivatives, and design of this study.

cacy was deemed insufficient to justify its use in such pathologies.^[23,26–29] Currently, EbSe is used in a clinical trial as substitute for lithium in the treatment of bipolar disorder^[29]. The mechanism via which EbSe mimics the action of lithium seems to be mediated by the interaction with the cysteinyl residue of IMPase, one of the enzymes that is targeted by lithium in the treatment of bipolar disorders.^[29]

EbSe can be reduced via interaction with different thiols.^[30–34] Though not studied systematically after *in vivo* administration of EbSe, the formation of adducts with the most abundant low-molecular containing thiol molecules (i.e., cysteine (Cys) and glutathione (GSH)) and also the oxidation of its reduced intermediate to Ebselen diselenide (EbSe)₂ are predictable (Figure 1).^[34] Several organoselenides can act as weak electrophiles,^[35,36] and can be oxidized to more reactive selenoxide intermediates via flavin-containing monooxygenases.^[37,38] Accordingly, EbSe and metabolites can be oxidized to organoselenoxides,^[37,38] which may serve as more potent inhibitors of thiol-containing enzymes.^[39]

Experimental and *in silico* studies have been carried out to find new Mpro and PLpro inhibitors, as well as, to explain the mechanisms of enzyme inhibition at the molecular and atomic level.^[23,40–43] Recent studies have suggested that EbSe interacts in the active site of the Mpro and PLpro and could react with the Cys145 and Cys111, respectively, leading to a Se–S bond formation, inhibiting the proteases, as previously demonstrated *in vitro*.^[9,22] In addition, an *in silico* study has indicated that EbSe can bind with high probability to a second binding site of Mpro, located between the II and III domains (residues: Gln107, Pro108, Ile200, Val202, His246, Phe294), besides the

catalytic site.^[40] However, there are no studies on the interaction of EbSe metabolites with SARS-CoV-2 proteases. The metabolism of EbSe has been scantily explored, but the available data indicate that it is methylated and glucuronylated to 2-methylselenobenzanilide (EbSe-Me), 4'-hydroxy-2-methylselenobenzanilide (EbSe-Me-OH), 2-(methylseleninyl)-N-phenylbenzamide (or methylebselenoxide, EbSeO-Me), 4'-glucuronyloxy-2-methylselenobenzanilide (EbSe-OGlcA), and 2-glucuronylselenobenzanilide (EbSe-SeGlcA), in addition to the formation 2,2'-diseleno-bis(benzanilide) (ebselen diselenide, EbSe)₂ (Figure 1).^[37,44–46] In addition, many putative metabolites and/or intermediates have been proposed, such as Cys- and GSH-adducts (EbSe-Cys and EbSe-GSH), monoxides (EbSeO and EbSeO-GSH), dioxides (EbSeO₂), selenenic- (EbSeOH) and seleninic acids (EbSeOOH).^[38,47,48] Thus, to better understand and predict the biological activity of organoselenium compounds, its metabolites need to be taken into account.

Importantly, a relation between selenium and COVID-19 has been demonstrated in some studies. According to Zhang *et al.*, a positive linear association between Se status and the cure rate of patients with COVID-19 was observed in Chinese cities.^[49] Moghaddam *et al.*, showed that the serum concentration of Se and selenoproteins was significantly lower in patients with COVID-19 than in healthy controls. Furthermore, the Se status in surviving patients was significantly higher than in non-survivors.^[50] This evidence suggests that Se compounds may have a role in prevention and therapy of COVID-19. Of particular importance, it has been suggested that metabolites of the

inorganic pool of selenium may inhibit the Mpro from SARS-CoV-2.^[25]

Here, in this study, we expand the study of EbSe interaction with the Mpro and PLpro from SARS-CoV-2. Besides the EbSe, its putative metabolites (Figure 1) were considered as molecules potentially involved in the enzymatic inhibition. The comparison of EbSe and its putative metabolites based on their *in silico* interactions with the two proteases of SARS-CoV-2 can help to explain the apparent higher potency of EbSe as inhibitor of Mpro than of PLpro.^[24] Here, we have also studied *in silico* the interaction of ethaselen (EthSe), an analog of ebselen, which is currently under clinical trial for the treatment of non-small cell lung carcinoma with thioredoxin reductase (TrxR) high expression (ClinicalTrials.gov Identifier: NCT02166242).^[51,52] Further, we have studied the interaction of the simplest among the diaryl diselenides (diphenyl diselenide, DPDSe) because this drug shares some chemical and pharmacological properties with EbSe. For instance, both can inhibit thiol-containing enzymes.^[32,53] In contrast to EbSe, DPDSe can be metabolized to inorganic selenium and feed the inorganic selenium pool.^[32] Consequently, DPDSe could also impair SARS-CoV-2 pathology by forming metabolites that can inhibit virus proteases and by promoting selenoproteins biosynthesis.^[25] In the past, DPDSe was also tested in a very small clinical trial and did not cause acute toxicity.^[54]

The interaction of EbSe and its metabolites with the active site of Mpro and PLpro, and the Zn site from PLpro has been extensively studied by molecular docking simulation (Figure 1 and Figure 2). In addition, DFT calculations were carried out to better characterize the reaction between EbSe and Cys residues using a simple molecular model, i. e. methylthiol in place of the Cys.

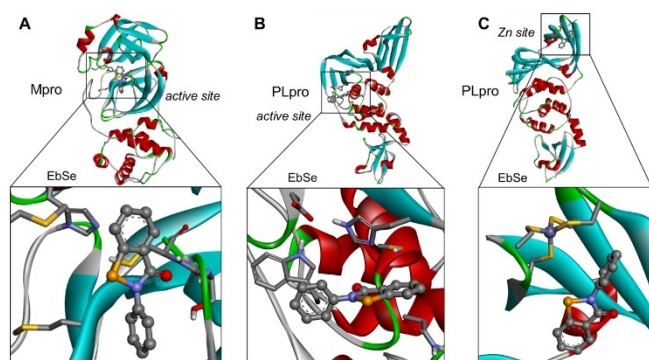


Figure 2. Docking simulations between Mpro active site (A), PLpro active site (B), and PLpro Zn site (C) with EbSe. EbSe conformer with the largest negative ΔG is shown.

2 Materials and Methods

2.1 Docking Simulations

AutoDock Vina was used for the docking simulations,^[55] with exhaustiveness of 50. The Mpro and PLpro crystallographic structures were obtained from the Protein Data Bank (PDB) with the codes 6LU7 and 7JN2, respectively. Non-essential waters, ions, ligands, and other molecules were removed from the X-ray protein structures, while the hydrogens were added using the CHIMERA program, followed by 100 steps of energy minimization (amberff99SB).^[56] The Mpro gridbox was centered on the active site (-14.04, 17.44, 66.22) with the size $25 \times 35 \times 25$ Å (spacing 1 Å), obtaining a redocking of 2.1 Å. For the PLpro, the redocking (0.63 Å) was obtained with the grid box on the coordinates 44.24, 30.68, and 1.66 (size: $24 \times 20 \times 20$ Å). However, few EbSe conformers interacted with the Cys111 (PLpro). In fact, the co-crystallized ligand does not interact with the PLpro catalytic triad.^[57] To improve the interactions with the PLpro active site residues, the grid box was shifted. Now, the PLpro docking was centered on the active site (39.64, 30.68, 1.66; size: $20 \times 20 \times 20$ Å), besides the Zn binding site ($82.40 \times 26.32 \times -0.62$; size: $20 \times 20 \times 20$ Å). The tridimensional model of ebselen and its metabolites and derivatives were created with Avogadro and MOPAC (PM6 method),^[58–60] taking into account the physiological pH (7.4). For comparison, the analog of Ebselen containing sulfur, also known as PZ-25 (ebsulfur),^[61] was also studied. Monoxides and the seleninic acid were considered as *R*, *S*-isomers because the Se nucleus oxidation creates a chiral center on Se. For each molecule, the 20 best conformers (in terms of ΔG) were analyzed in the Discovery Studio Visualizer Dassault Systèmes). The details of interaction of ebselen and derivatives were analyzed for the conformers with the largest negative binding energy (ΔG) and conformers which displayed the best interaction of selenium atom with the sulfur atom of Cys residues of the active site of Mpro and PLpro. Specifically, the distance between the Se atom to S atom was considered an indicator of potential covalent bond formation between Ebselen and its metabolites with the enzymes.

In addition, covalent docking studies were carried using the AutoDock 4 software (Lamarckian Genetic Algorithm) with the flexible side chain method.^[62,63] The ideal chemical geometry of modified Cys residue (Cys + EbSe adduct) was obtained by the optimization (PM6 method) of a cluster containing the main residues around the EbSe molecule. The Cys + EbSe was considered as a modified residue in the protein structures, and its side chain was treated as flexible. The grid boxes (spacing 0.375 Å, and size: $75 \times 75 \times 75$ Å) were centered on the previously cited coordinates.

2.2 DFT Calculations

All Density Functional Theory (DFT) calculations were done with ORCA 4.1.2.^[64,65] Energy optimizations and vibrational frequency calculations were conducted without any constraints using OPBE GGA functional^[66] at a level of theory here denoted as ZORA-OPBE/ZORA-def2-TZVP. Scalar relativistic effects were included using the zeroth-order regular approximation (ZORA).^[67] This level of theory was benchmarked^[68] and successfully used for structural and energy description of organochalcogenides.^[68–71] Using the vibrational frequency calculations, all optimized geometries were confirmed to be minima with no imaginary frequency, or transition states (TS) (with a single imaginary frequency corresponding to correct normal mode). The transition state was initially located on the PES using the Nudged Elastic Band (NEB) approach^[72] as implemented in the ORCA suite.

3 Results and Discussion

For optimal presentation of the results, the docking data of EbSe, EbSe₂, EthSe, and DPDS_e are presented in the main article, while EbSe-Me, EbSe-MeOH, EbSeO-Me-(R), EbSeO-Me-(S), EbSe-OGlcA, EbSe-SeGlcA, EbSe-Cys, EbSe-GSH, EbSeO-GSH-(R), EbSeO-GSH-(S), EbSeO-(R), EbSeO-(S), EbSeO₂, EbSeOOH-(R), EbSeOOH-(S), EbSeOH, and PZ-25 are shown in the Supporting information.

3.1 EbSe Interactions with Mpro Active Site

The Mpro catalytic site lies between the I and II domains and is formed by a dyad Cys145 and His41. The active pocket is composed of Phe140, Leu141, Asn142, Gly143, Ser144, Met165, Glu166, Gln189, and Thr190. The catalytic dyad has two nucleophilic sites (in the imidazole of His41 and the thiol of Cys145) that can attack electrophilic sites on drugs.^[9,11,40,73,74]

The docking simulations of the Mpro active site indicated that, energetically, EbSe-SeGlcA and EbSe₂ possess the largest negative binding energies (−9.0 and −9.4 kcal.mol^{−1}), while the DPDS_e and EbSe-Me show the least negative ΔG values among the tested compounds (−6.1 and −6.2 kcal.mol^{−1}) (Table 1). Generically, the ligands showed interaction distances Se⋯SH ranging from 3.0 to 5.6 Å while the O=C⋯SH distances vary in range from 3.3 to 5.4 Å (Table S1). This suggests the possibility of a covalent bond formation with the active site cysteine of Mpro, which can form adducts that impair the functions of the enzyme. The feasibility of a covalent bond formation between Ebs-Se-S-Cys145 was further indicated by DFT calculations and covalent docking analysis (Supporting Information). As demonstrated for disulfiram, the chalcogen interaction with the catalytic thiol group of Mpro is essential for potential covalent interaction.^[74] The molecules' conformers with the

Table 1. Binding free energy (ΔG , kcal.mol^{−1}) and interaction distances between EbSe, its metabolites and derivatives with the –SH group of cysteinyl (Cys145) from the active site of SARS-CoV-2 Main Protease (Mpro). Data from the rigid docking.

Molecule	ΔG^*	dist. (Å)	interact.	ΔG^{**}	dist. (Å)	interact.
EbSe	−6.5	3.3	C=O	−5.4	4.1	Se
EbSe-Me	−6.2	4.7	C=O	−5.9	3.8	Se
EbSe-Me-OH	−6.6	3.9	Se	−6.0	3.8	Se
EbSeO-Me-(R)	−6.6	4.6	C=O	−6.5	3.4	Se
EbSeO-Me-(S)	−6.8	3.8	Se	−5.8	3.8	Se
EbSe-OGlcA	−7.3	–	–	−6.5	4.6	Se
EbSe-SeGlcA	−9.0	–	–	−7.4	4.1	Se
EbSe ₂	−9.4	3.5	C=O	−7.7	3.9	Se
EbSe-Cys	−7.4	3.9	S	−6.9	3.8	Se
EbSe-GSH	−8.1	4.2	Se	−7.5	4.4	Se
EbSeO-GSH-(R)	−7.9	4.1	C=O	−7.2	3.8	Se
EbSeO-GSH-(S)	−8.6	3.5	C=O	−7.2	3.6	Se
EbSeO-(R)	−6.7	3.5	C=O	−5.4	3.9	Se
EbSeO-(S)	−6.7	3.3	C=O	−5.4	3.0	Se
EbSeO ₂	−7.1	3.3	C=O	−5.0	4.2	Se
EbSeOOH-(R)	−6.6	4.6	Se	−5.8	3.6	Se
EbSeOOH-(S)	−6.7	4.2	C=O	−6.6	4.0	Se
EbSeOH	−6.5	4.6	Se	−5.7	3.7	Se
EthSe	−7.0	3.6	C=O	−6.7	4.6	Se
PZ-25	−6.5	3.3	C=O	−5.2	3.5	S
DPDS _e	−6.1	4.4	Se	−5.0	4.3	Se

* Lowest binding energy (kcal.mol^{−1}); ** Conformers with an adequate interaction with Cys (kcal.mol^{−1}); Binding energies and distances (from Cys) were analyzed. The colors (heatmap) indicate how favorable the ligand-enzyme interaction is. Green, yellow, and red colors indicate a favorable, intermediate, and less favorable interaction, respectively.

largest negative ΔG interacted with Cys145 by C=O and Se groups, which are the two main electrophilic sites of EbSe, its metabolites, and derivatives. EbSe, EbSeO-(S), EbSeO₂, and PZ-25 showed the shortest interaction distance (3.3 Å) between the electrophilic carbon in the amide carbonyl moiety (C=O) and the thiol group of Cys145, whereas the EbSeO-(S) and EbSeO-Me-(R) had the lowest interaction distance Se⋯SH (3.0 and 3.4 Å, respectively). The similar interactions of EbSe and ebsulfur (PZ-25) could indicate alike activities.

The ligands presented hydrophobic interactions (mainly with His41, Met49, and Met165) and hydrogen bonds (with Ser144 and Cys145) within the Mpro pocket, which could increase the stabilization of the receptor-ligand complex (Table 1 and S1). The π -stacking interaction between His41 and EbSe is in agreement with the data by Cozza.^[23] In addition, the hydrophobic interaction with Met49, His41, and Met165 residues,^[75–77] and H-bonds with Ser144^[78,79] plays an important role in the inhibitor-enzyme complex stabilization in SARS-CoV-2 Mpro.

The conformers with the largest negative binding energies of EbSe, EbSe₂, and EthSe showed an interaction between the carbon atom in the amide carbonyl group and the thiol from the Cys145 (O=C⋯SH). The DPDS_e, which

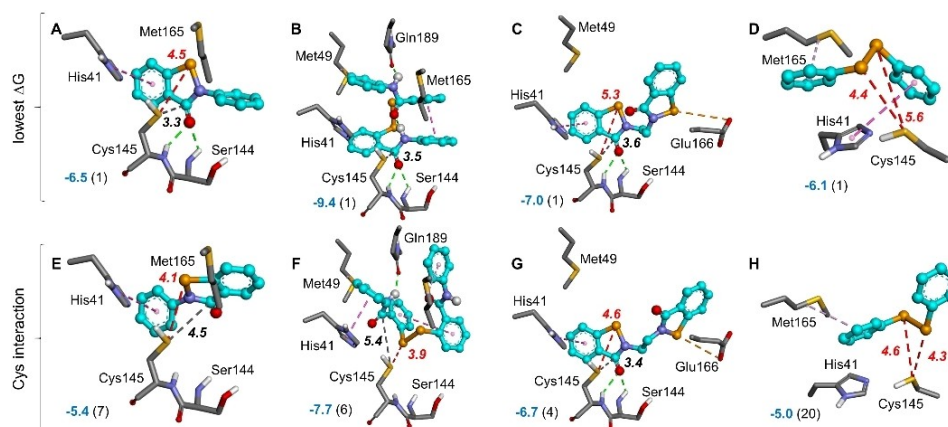


Figure 3. Protein-rigid docking between Mpro and organoselenium compounds. EbSe (A, E), EbSe₂ (B, F), EthSe (C, G), and DPDSe (D, H) are shown using the ball and stick representation (carbon atoms in cyan color), while the main amino acid residues involved in the interaction are shown using the stick representation. A–D are the cases with the largest negative ΔG , whereas the E–H are the conformers with the best interaction between the S atom of Cys and the Se atom of the tested compounds. The distances (\AA) of the O=C...S and Se...S interactions are shown in black and red colors, respectively. The binding free energy, ΔG (kcal.mol^{-1}), is shown in blue color and the conformer number is given in parenthesis. H-bonds, hydrophobic, O=C...S, and Se...S interactions are represented using green, purple, grey and red dashed lines, respectively.

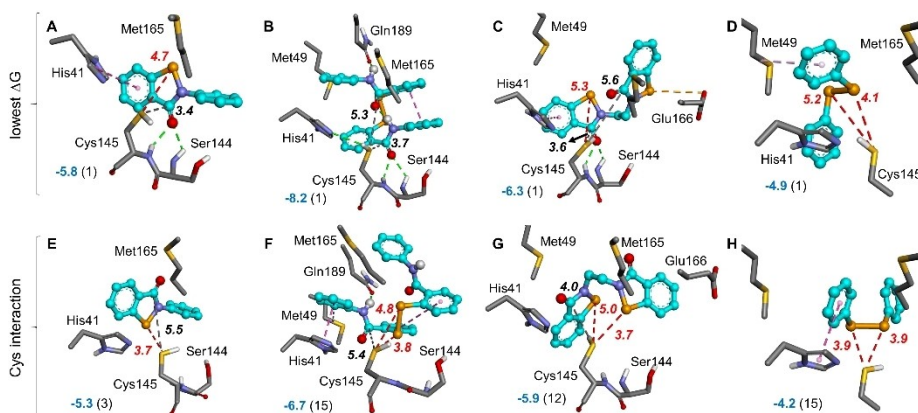


Figure 4. Flexible docking between Mpro and organoselenium compounds. EbSe (A, E), EbSe₂ (B, F), EthSe (C, G), and DPDSe (D, H) are shown using the ball and stick representation (carbon atoms in cyan color), while the flexible residues Cys145 and His41 are shown using the stick representation. A–D are the cases with the largest negative ΔG , whereas the E–H are the conformers with the best interaction between the S atom of Cys and the Se atom of the tested compounds. The distances (\AA) of the O=C...S and Se...S interactions are shown in black and red colors, respectively. Binding free energy, ΔG (kcal.mol^{-1}), is shown in blue color and the conformer number is given in parenthesis. H-bonds, hydrophobic, O=C...S, and Se...S interactions are represented using green, purple, grey and red dashed lines, respectively.

does not have the C=O moiety, shows a Se...SH interaction with Cys145 (Figure 3A–D). The analysis of the conformers with the suitable Cys145 interaction indicates that the Se moiety from EbSe, EbSe₂, EthSe, and DPDSe could be a target for the nucleophilic attack from S of Cys145 residue (3.9–4.6 \AA) (Figure 3E–H).

To better understand the interactions between the ligands and the Mpro active site, the side chains of the catalytic dyad (Cys145 and His41) were allowed to rotate, i.e., they were left flexible. The conformers of EbSe and EthSe with the largest negative binding energy show O=C...

SH and Se...SH interactions with Cys145, while EbSe₂ present only the O=C...SH interaction (Figure 4A–D). The conformers of EbSe, EbSe₂, EthSe and DPDSe with a suitable interaction with the Cys145 show a Se...SH interaction distance in the range of 3.7 to 3.9 \AA , indicating possible nucleophilic attack from the thiol to selenium. In addition, EbSe, EbSe₂, and EthSe present O=C...SH interactions. However, the distances of the electrophilic C=O (ranging from 4.0 to 5.5 \AA) are longer than those associated with the Se...SH interaction (Figure 4E–H).

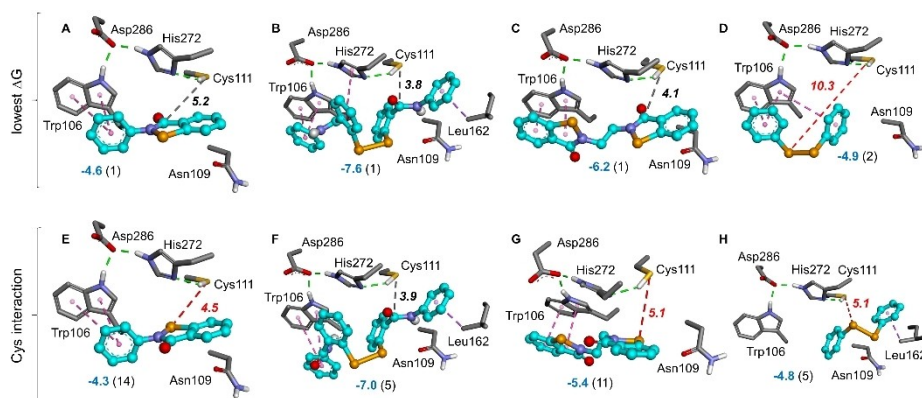


Figure 5. Protein-rigid docking between PLpro and organoselenium compounds. EbSe (A, E), EbSe)₂ (B, F), EthSe (C, G), and DPDSe (D, H) are shown using the ball and stick representation (carbon atoms in cyan color), while the main amino acid residues involved in the interactions are shown using the stick representation. A–D are the cases with the largest negative ΔG , whereas the E–H are the conformers with the best interaction between the S atom of Cys and the Se atom of the tested compounds. The distances (\AA) of the $\text{O}=\text{C}\cdots\text{S}$ and $\text{Se}\cdots\text{S}$ interactions are shown in black and red colors, respectively. Binding free energy, ΔG ($\text{kcal}\cdot\text{mol}^{-1}$), is shown in blue color and the conformer number is given in parenthesis. H-bonds, hydrophobic, $\text{O}=\text{C}\cdots\text{S}$, and $\text{Se}\cdots\text{S}$ interactions are represented using green, purple, grey and red dashed lines, respectively.

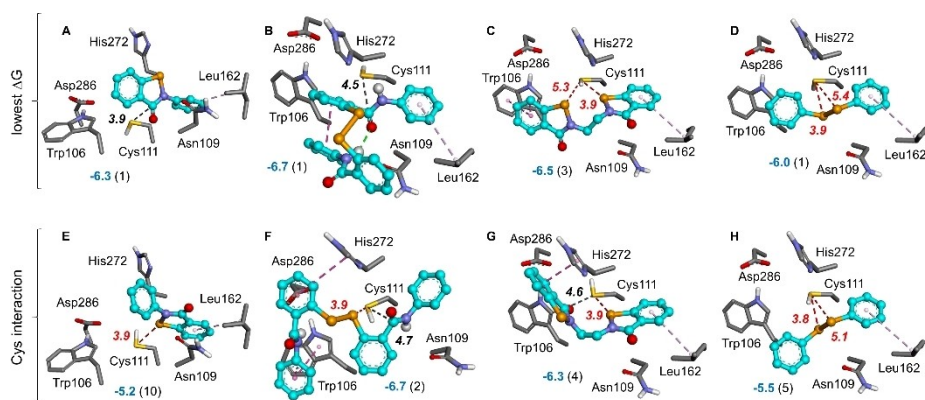


Figure 6. Flexible docking between PLpro and organoselenium compounds. EbSe (A, E), EbSe)₂ (B, F), EthSe (C, G), and DPDSe (D, H) are shown using the ball and stick representation (carbon atoms in cyan color), while the flexible residues Cys111, His272, and Asp286 are shown using the stick representation. A–D are the cases with the largest negative ΔG , whereas the E–H are the conformers with the best interaction between the S atom of Cys and the Se atom of the tested compounds. The distances (\AA) of the $\text{O}=\text{C}\cdots\text{S}$ and $\text{Se}\cdots\text{S}$ interactions are shown in black and red colors, respectively. Binding free energy, ΔG ($\text{kcal}\cdot\text{mol}^{-1}$), is shown in blue color and the conformer number is given in parenthesis. H-bonds, hydrophobic, $\text{O}=\text{C}\cdots\text{S}$, and $\text{Se}\cdots\text{S}$ interactions are represented using green, purple, grey and red dashed lines, respectively.

Comparison among the conformers of EbSe, EbSe)₂, EthSe, and DPDSe with the largest negative binding free energy (ΔG), both in the rigid and flexible docking, indicated that the rigid docking (Figure 3) affords more thermodynamically favorable values than the flexible docking with Mpro (Figure 4), and presents a larger number of interactions with the amino acid residues of the catalytic pocket, mainly Ser144, Gln189, and Gly143. EbSe, EbSe)₂, EthSe and DPDSe show closer interactions between electrophilic (Se and $\text{C}=\text{O}$, from ligands) and nucleophilic (HS-Cys145, from Mpro) sites.

3.2 EbSe Interactions with PLpro Active Site

The active site of PLpro from SARS-CoV-2 possesses a catalytic triad, composed of Cys111, His272, and Asp286 residues, where the Cys111 acts as the critical nucleophile in the cleavage of the peptide bond from the pp1a and pp1ab. His272 and Asp286 act as an acid-base pair helping to promote the Cys111 deprotonation.^[80–82] The docking simulations were focused on this region (Figures 5 and 6, Tables 2 and S2). EbSe-GSH and EbSe)₂ showed the largest negative binding energies (-7.5 and -7.6 $\text{kcal}\cdot\text{mol}^{-1}$), while EbSeO-(R), DPDSe, and PZ-25 showed the least negative ΔG values of tested compounds (-4.9 and -4.7 $\text{kcal}\cdot\text{mol}^{-1}$). In

Table 2. Binding free energy (ΔG , kcal.mol⁻¹) and interaction distance between EbSe metabolites and derivatives and the -SH group of cysteinyl (Cys111) from the active site of SARS-CoV-2 Papain-Like Protease (PLpro). Data from the rigid docking.

Molecule	ΔG^*	dist. (Å)	interact.	ΔG^{**}	dist. (Å)	interact.
EbSe	-6.1	5.2	C=O	-4.3	4.5	Se
EbSe-Me	-5.2	4.0	C=O	-4.7	4.3	Se
EbSe-Me-OH	-5.2	3.9	C=O	-5.1	4.3	Se
EbSeO-Me-(R)	-4.9	4.0	C=O	-4.7	4.9	Se
EbSeO-Me-(S)	-5.3	3.9	C=O	-4.6	5.6	Se
EbSe-OGlcA	-6.3	-	-	-5.8	-	-
EbSe-SeGlcA	-6.1	-	-	-5.7	3.9	C=O
EbSe) ₂	-7.6	3.8	C=O	-7.0	3.9	C=O
EbSe-Cys	-5.9	3.8	C=O	-5.1	5.0	Se
EbSe-GSH	-7.5	3.9	C=O'	-7.0	3.9	C=O'
EbSeO-GSH-(R)	-7.0	3.9	C=O'	-6.8	3.9	C=O'
EbSeO-GSH-(S)	-5.9	-	-	-5.7	4.1	C=O'
EbSeO-(R)	-4.9	-	-	-4.5	5.1	Se
EbSeO-(S)	-5.0	-	-	-4.2	5.4	C=O
EbSeO ₂	-5.4	-	-	-4.9	5.0	Se
EbSeOOH-(R)	-5.1	-	-	-4.3	5.0	Se
EbSeOOH-(S)	-5.4	3.9	C=O	-4.7	5.0	Se
EbSeOH	-5.1	3.9	C=O	-4.4	5.0	C=O
EthSe	-6.2	4.1	C=O	-5.4	5.1	Se
PZ-25	-4.7	5.0	C=O	-4.4	4.9	S
DPDSe	-4.9	-	-	-4.8	5.1	Se

* Largest negative binding energy (kcal.mol⁻¹); ** Conformers with an adequate interaction with Cys(kcal.mol⁻¹); ' indicates the C=O group from peptide moieties of GSH. Binding energies and distances (from Cys) were analyzed. The colors (heatmap) indicate how favorable the ligand-enzyme interaction is. Green, yellow, and red colors indicate a favorable, intermediate, and less favorable interaction, respectively.

general, the conformers with the largest negative ΔG interact with the catalytic Cys111 via the electrophilic carbon atom of the C=O group in the amide bond, whereas some conformers with less negative ΔG present an adequate interaction with Se (Table 2).

The conformers of EbSe, EbSe)₂, and EthSe with the largest negative binding energy showed interaction between the amide carbonyl and the thiol groups (O=C...SH) from the organoselenium molecule and Cys111. However, the DPDSe does not interact with the SH group of Cys111 (Figure 5A–D). On the other hand, the conformers with the best Se...SH-Cys111 interaction demonstrated that the EbSe, EthSe, and DPDSe interact with the Cys by Se...SH interaction (4.5–5.1 Å), while EbSe)₂ is the only form that interacts with the electrophilic C of the amide carbonyl group (O=C) (Figure 5E–H). In addition, we observed hydrophobic interactions between Trp106, Leu162, and His272 of PLpro with the ligands. These residues can play an important role in stabilizing the PLpro-ligand complexes, as previously reported.^[81,83,84]

In addition, the rigid docking (considering the cases with the largest negative ΔG and with a suitably good distance from the -SH of Cys111) with the other EbSe

metabolites and derivatives demonstrates that the conformers of EbSe-SeGlcA, EbSeO-(S), and EbSe-OH interact predominantly with the carbonyl moiety of the amide bond of the *N*-phenylbenzamide group, while EbSe-GSH, EbSe-GSH-(R), and EbSe-GSH-(S) interact with the carbonyl of the peptide bond of the GSH moiety (Table S2). EbSeO-(R) and EbSeO₂ showed a Se...SH interactions, whereas EbSe-Me, EbSe-Me-OH, EbSeO-Me-(R), EbSeO-Me-(S), EbSe-Cys, EbSeOOH-(R), and EbSeOOH-(S) interacted with the active site of PLpro both via Se...SH and O=C...SH interactions. The glucuronic acid metabolite EbSe-OGlcA interacted with the SH moiety of Cys111 and the α -carbon of the sugar. The sulfur derivative of EbSe, the PZ-25, showed interactions similar to EbSe, interacting with the -SH by S and C=O groups (Table S2).

The flexible docking of PLpro, which takes into account the flexibility of the side chains of the catalytic triad (Cys111, His272, and Asp286), was also carried out to better understand the interaction of the ligands with the active site of PLpro. The conformers with the largest negative binding energy of EbSe and EbSe)₂ demonstrated a O=C...SH interaction with the Cys111, while the EthSe and DPDSe presented Se...SH interactions (Figure 6A–D). The conformers of EbSe, EbSe)₂, EthSe and DPDSe molecules, with an adequate interaction with the Cys111 (i.e., the shortest distance), showed a Se...SH interaction at a distance of ~3.9 Å, indicating a possible nucleophilic attack from the thiol to selenium. EbSe)₂ and EthSe also presented a O=C...SH interaction; however, the distance (~4.6 Å) was higher than that associated to the Se...SH interaction (Figure 6E–H). With exception of EbSe)₂, the binding free energy (ΔG) of EbSe, EthSe, and DPDSe was negatively larger (thermodynamically more favorable) in the PLpro flexible docking than the rigid docking. In contrast to the findings with Mpro, in the docking with flexible PLpro catalytic triad, the formation of the complexes of the ligands with the enzyme is more energetically favorable compared to the rigid docking. Notably, the interaction distances for both Mpro and PLpro in the flexible docking indicate stronger interactions between the ligands and the enzymes than in the rigid docking (Table S4).

3.3 EbSe Interactions with PLpro Zn Site

The Zn site of PLpro presents a Zn(II) ion bound to four Cys residues (namely: Cys189, Cys192, Cys224, and Cys226), which is similar to other cysteine-rich motifs found in many proteins, such as zinc finger proteins,^[85,86] butyrobetaine hydroxylase,^[87,88] metallothionein,^[89,90] and 5-aminolevulinic acid dehydratase (δ -AlaD).^[91,92] This motif plays an important structural and catalytic role in many proteins, indicating a potential molecular target for therapeutic intervention. Consequently, the disruption of protein function via organochalcogen mediated oxidation of cysteinyl residues

in the Zn-binding site of PLpro deserves to be investigated in greater detail.

Based on the free binding energies, EbSe-OGlcA (-6.0 kcal.mol $^{-1}$), EbSe $_2$ (-5.7 kcal.mol $^{-1}$), and EbSeO $_2$ presented the most favorable values (-5.7 kcal.mol $^{-1}$), while EbSeO-GSH-(R) and EbSe-OH showed the highest (-5.0 kcal.mol $^{-1}$ for both). Generally, the conformers with the largest negative ΔG interacted with the thiolate ($-S^-$) of Cys224, via the electrophilic carbon (C=O) of the amide bond and/or the Se center of EbSe or its metabolites. However, other conformations, with less favorable interaction energies, presented adequate interactions with $-S^-$ from Cys192 and the Se moiety (Table 3 and S3). EbSe, its

Table 3. Binding free energy (ΔG , kcal.mol $^{-1}$) and interaction distance between EbSe, its metabolites and derivatives with the $-S^-$ group of Cys residues from the Zn site of SARS-CoV-2 Papain-Like Protease (PLpro). Data from the rigid docking.

Molecule	ΔG^*	dist. (Å)	interact.	ΔG^{**}	dist. (Å)	interact.
EbSe	-5.3	3.9	Se ^a	-4.1	3.8	Se ^b
EbSe-Me	-5.4	4.6	C=O ^a	-4.7	4.1	Se ^b
EbSe-Me-OH	-5.6	4.6	C=O ^a	-4.8	4.1	Se ^b
EbSeO-Me-(R)	-5.3	3.8	C=O ^a	-4.6	4.0	Se ^b
EbSeO-Me-(S)	-5.2	4.3	C=O ^a	-4.7	4.1	Se ^b
EbSe-OGlcA	-6.0	-	-	-5.2	4.2	Se ^b
EbSe-SeGlcA	-5.4	3.8	C=O ^a	-4.8	4.0	Se ^b
EbSe $_2$	-5.7	-	-	-5.0	4.2	Se ^b
EbSe-Cys	-5.5	5.4	C=O ^a	-4.9	4.3	Se ^b
EbSe-GSH	-5.4	4.2	C=O ^a	-4.7	4.7	Se ^b
EbSeO-GSH-(R)	-5.0	4.3	C=O ^b	-4.7	4.7	Se ^b
EbSeO-GSH-(S)	-5.5	4.6	C=O ^a	-5.1	4.1	Se ^b
EbSeO-(R)	-5.6	3.8	Se ^a	-4.9	4.0	Se ^a
EbSeO-(S)	-5.3	4.1	Se ^a	-4.2	4.0	Se ^b
EbSeO $_2$	-5.7	4.1	Se ^a	-4.6	4.5	Se ^b
EbSeOOH-(R)	-5.2	4.4	C=O ^a	-4.9	4.3	Se ^b
EbSeOOH-(S)	-5.3	4.3	C=O ^a	-5.0	4.3	Se ^b
EbSeOH	-5.0	3.8	C=O ^a	-4.8	4.0	Se ^b
EthSe	-5.4	4.2	Se ^a	-5.0	4.7	Se ^b
PZ-25	-5.3	3.9	S ^a	-4.2	4.0	S ^b
DPDSe	-5.6	4.1	Se ^a	-5.1	4.1	Se ^b

* Largest negative binding energy (kcal.mol $^{-1}$); ** Conformers with an adequate interaction with Cys (kcal.mol $^{-1}$); ' indicates the C=O group from peptide moieties of GSH. Binding energies and distances (from Cys) were analyzed. The colors (heatmap) indicate how favorable the ligand-enzyme interaction is. Green, yellow, and red colors indicate a favorable, intermediate, and less favorable interaction, respectively. ^a $-S^-$ from Cys224; ^b $-S^-$ from Cys192.

metabolites and derivatives showed Se \cdots SH interactions at a distance ranging from 3.8 to 4.7 Å, while the O=C \cdots SH interactions fell in the range from 3.8 to 5.4 Å. Thus, the possibility of forming a covalent bond between the cysteine and the ligands may contribute to a possible inhibition of the enzyme via disruption of the Zn site in PLpro (Table S3).

The docking simulations demonstrated that the conformers with the largest negative ΔG of EbSe, EthSe, and DPDSe could interact with the thiolate group of Cys224

residue via Se (3.9 to 4.1 Å), while EbSe $_2$ does not interact with the Cys residues (Figure 7A–D). Furthermore, these molecules can also interact with the Cys192 residue, as the docking demonstrated that EbSe, EbSe $_2$, EthSe, and DPDSe can interact with PLpro thiolate group in the Zn-site (3.8 to 4.7 Å) (Figure 7E–H).

These observations indicate that the Zn site from PLpro may also be a target for potential drugs. Indeed, the Cys residues could attack the organoselenium molecules either at Se or at the electrophilic carbon in the C=O group. In fact, the organoselenium molecules are able to interact with cysteine-rich motifs and inhibit proteins, as observed for metallothionein,^[93] butyrobetaine hydroxylase,^[87] δ -AlaD,^[94,95] and zinc finger proteins.^[96] Alternatively, a recent study by Sargsyan *et al.*,^[22] demonstrated that the clinically safe drugs, EbSe and disulfiram, could covalently bind to the cysteinyl residues in the Zn site of PLpro of SARS-CoV-2, and caused the ejection of the zinc ion due to a covalent adduct formation with cysteinyl residues.

3.4 DFT Calculations: Cys Attack to EbSe

Accurate energetics calculations were carried out on a model molecular system formed by EbSe and methylthiol, aiming at verifying the possibilities of attack at selenium and at carbonyl, respectively (Table 4). The former is energetically favored

Table 4. Energies (kcal.mol $^{-1}$) relative to the reactants of the nucleophilic attack at Se atom. Level of theory ZORA-OPBE/ZORA-def2-TZVP.

	Se	C=O
Reactants	0.00	0.00
Transition State (TS)	41.03	-
Product	-13.40	13.11

($\Delta E = -13.40$ kcal.mol $^{-1}$), while the latter is not ($\Delta E = +13.11$ kcal.mol $^{-1}$). This immediately suggests the peculiar role of selenium, the presence of which allows not only a mere interaction, but a reaction can effectively take place with the formation of a S–Se bond. From our docking results it is also clear that EbSe has a suitable molecular geometry to approach the target cysteine and promote this reaction. The activation energy, computed with respect to the free reactants, is 41.03 kcal.mol $^{-1}$. A single synchronous step has been postulated and located on the potential energy surface (PES). This is consistent with the mechanistic analysis reported by Bayse,^[48] although a significantly lower activation energy has been reported due to the presence of explicit water molecules mediating the proton transfer from sulfur to nitrogen. The optimized geometries of the reactants, transition state and product are shown in Figure 8. These DFT results corroborate other literature data.^[96–100]

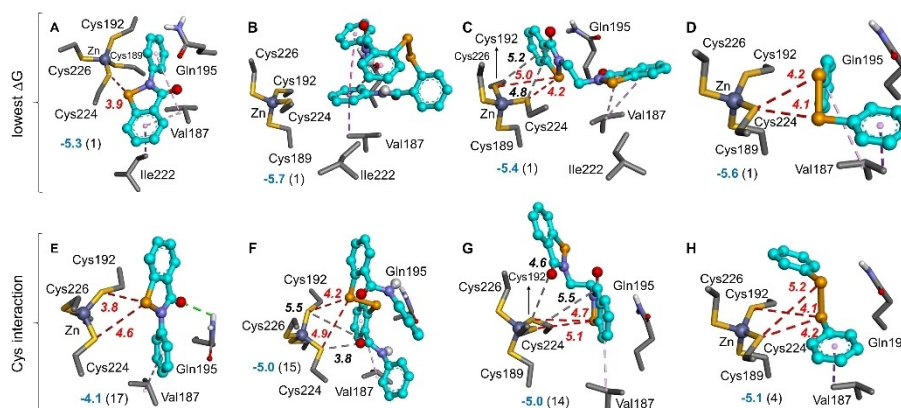


Figure 7. Protein-rigid docking between PLpro (Zn site) and organoselenium compounds. EbSe (A, E), EbSe₂ (B, F), EthSe (C, G), and DPDSe (D, H) are shown using the ball and stick representation (carbon atoms in cyan color), while the main amino acid residues are shown using the stick representation. A–D are the cases with the largest negative ΔG , whereas the E–H are the conformers with the best interaction between the S atom of Cys and the Se atom of the tested compounds. The distances (Å) of the O=C...S and Se...S interactions are shown in black and red colors, respectively. Binding free energy, ΔG (kcal.mol⁻¹), is shown in blue color and the conformer number is given in parenthesis. H-bonds, hydrophobic, O=C...S, and Se...S interactions are represented using green, purple, grey and red dashed lines, respectively.

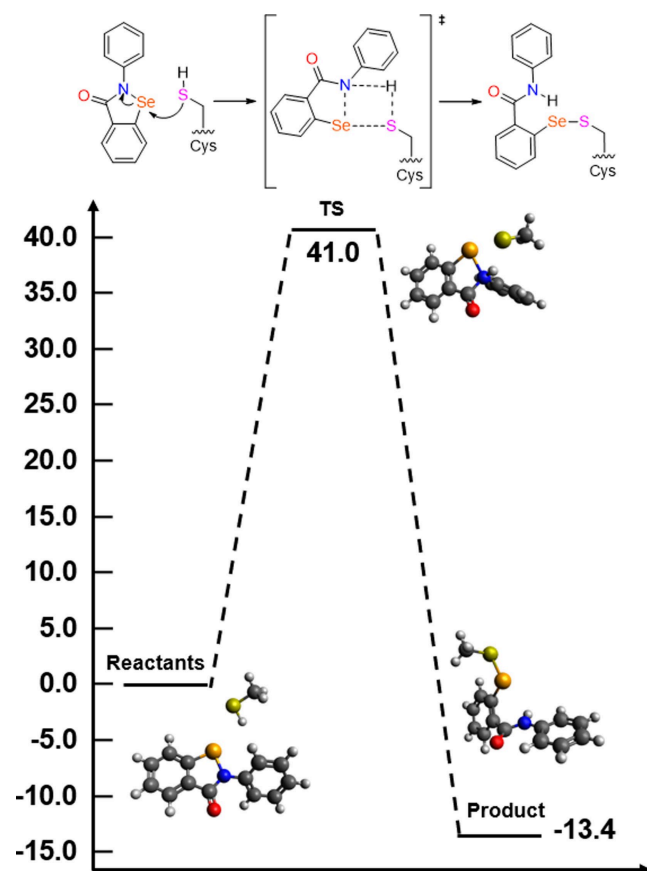


Figure 8. Concerted mechanism of SARS-CoV-2 MPro/PLpro Cys nucleophilic attack at selenium on Ebselen. Level of theory ZORA-OPBE/ZORA-def2-TZVP.

EbSe adduct with the Cys residues from the active site of Mpro and PLpro could be adequately accommodated in the enzymes' pocket, as demonstrated by the covalent docking^[62,63] (Figure S1), interrupting the binding and hydrolysis of the natural substrates (pp1a and pp1ab polyproteins), and inhibiting the viral proteases.

4 Conclusions

Our investigation on the interactions of EbSe, its metabolites and derivatives with the SARS-CoV-2 Mpro and PLpro reactive sites sheds novel insight into the possible enzyme's mechanism of inhibition. Docking simulations demonstrated that organoselenium compounds can effectively interact with the active site of Mpro and PLpro with suitable conformations which could lead to covalent adduct formation. The EbSe metabolite EbSe₂ seems to be a promising inhibitor of both Mpro and PLpro, due its negatively large ΔG values and Cys interactions. EthSe showed protein interactions similar to EbSe, suggesting that this molecule also could be a potential Mpro/PLpro inhibitor. However, *in vitro* studies are necessary to confirm these hypotheses. Furthermore, we highlight that the metabolites of the main ligands should also be considered in the docking simulations, because they can lead to a better understanding of the drug mechanism of action. The structural data obtained with metabolites can be used for the design of new drugs.

In our results, the interaction of EbSe, its metabolites, and derivatives indicated more favorable binding energies with the active site of Mpro than with the sites of PLpro. In agreement, Zmudzinski *et al.*, reported that EbSe and its derivatives *in vitro* inhibited SARS-CoV-2 Mpro more effi-

ciently than PLpro.^[41] All the tested molecules were able to interact with the catalytic Cys residue from Mpro and PLpro, by C=O and/or Se groups. Thus, they can potentially undergo nucleophilic attacks from Cys(111 or 145), and consequently, inhibit Mpro and PLpro by different mechanisms.

We have investigated the energetics for preferred nucleophilic attack of Cys-SH of SARS-CoV-2 Mpro/PLpro models on Ebselen using DFT calculations. Our findings suggest that the inhibition of SARS-CoV-2 possibly occurs via the nucleophilic attack of cysteinyl residues from protease to the Se atom rather than to C=O of EbSe.

As demonstrated by Ma *et al.*,^[24] under reducing conditions (in presence of 1,4-dithiothreitol (DTT)), EbSe was not able to effectively inhibit SARS-CoV-2 Mpro. In addition, its well known that in the plasma EbSe is bonded to the reduced Cys of albumin and/or low-molecular-weight thiol molecules (i.e., Cys and GSH).^[32,101–103] In this respect, in the presence of thiol molecules (R-SH), the Se–N bond of EbSe is cleavage and the Se–S bond is formed giving the EbSe-SR molecule, which is the main form of EbSe in the cell, and probably have less antiviral activity. Docking simulations between the EbSe thiol-metabolites, i.e. EbSe-Cys and EbSe-GSH, and the SARS-CoV-2 proteases demonstrated that the Cys interactions also could occur. The Se···S interactions indicate that a ligand exchange reaction, a well known reaction,^[104,105] can occur leading to the Se–S bond formation with the viral proteases. However, the low inhibitory activity of EbSe thiol-metabolites might be due to the energetic profile of the Cys attack on the Se–S bond of the metabolite, which could be less favorable than the attack on the Se–N bond of EbSe. Nevertheless, further investigation is prompted to discuss this hypothesis, which is important to understand the true antiviral potential of EbSe and other organoselenium compounds.

In this sense, the data obtained herein confirm and extend the view that organoselenium molecules are an important class of compounds that should be further studied for their efficacy in inhibiting SARS-CoV-2 proteases. Furthermore, we suggest that ethaselen, ebselen diselenide, ebsulfur, and methylebselenoxide (which can be obtained from synthetic methodologies already described in the literature^[106–112]) should be tested *in vitro* as inhibitors of virus replication and its proteases.

Statement of Contribution

All authors have read and agreed to the published version of the manuscript. Conceptualization, supervision, methodology, validation, and project administration: P.A.N., L.O. and J.B.T.R.; formal analysis, investigation, and data curation: P.A.N., F.B.O., G.R.B. and C.P.D.; writing-original draft preparation: P.A.N., F.B.O., G.R.B. and C.P.D.; writing-review and editing: P.A.N., M.A., L.O. and J.B.T.R.

Acknowledgements

The authors would like to thank the financial support by Coordination for Improvement of Higher Education Personnel CAPES/ PROEX (n° 23038.005848/2018-31; n°0737/2018). P.A.N., G.R.B., C.P.D., and J.B.T.R. was funded by CAPES (Edital 09–88887.505377/2020-00); F.B.O. was funded by CAPES (Edital 88887.354370/2019-00). L.O. was funded by the Università degli Studi di Padova, thanks to the P-DiSC (BIRD2018-UNIPD) project MAD³S (Modeling Antioxidant Drugs: Design and Development of computer-aided molecular Systems). M.A. was supported in part by grants from the National Institute of Environmental Health Sciences (NIEHS) – R01ES10563 and NIEHS R01ES07331.

Conflict of Interest

None declared.

Data Availability Statement

The data that supports the findings of this study are available in the supplementary material of this article.

References

- [1] J. A. Siordia, *J. Clin. Virol.* **2020**, *127*, 104357.
- [2] R. T. Gandhi, J. B. Lynch, C. del Rio, *N. Engl. J. Med.* **2020**, *383*, 1757–1766.
- [3] D. A. Berlin, R. M. Gulick, F. J. Martinez, *N. Engl. J. Med.* **2020**, *383*, 2451–2460.
- [4] B. Hu, H. Guo, P. Zhou, Z.-L. Shi, *Nat. Rev. Microbiol.* **2020**, DOI 10.1038/s41579-020-00459-7.
- [5] G. U. Jeong, H. Song, G. Y. Yoon, D. Kim, Y. C. Kwon, *Front. Microbiol.* **2020**, *11*, 1723.
- [6] M. Z. Tay, C. M. Poh, L. Rénia, P. A. MacAry, L. F. P. Ng, *Nat. Rev. Immunol.* **2020**, *20*, 363–374.
- [7] H. Harapan, N. Itoh, A. Yufika, W. Winardi, S. Keam, H. Te, D. Megawati, Z. Hayati, A. L. Wagner, M. Mudatsir, *J. Infect. Public Health* **2020**, *13*, 667–673.
- [8] M. H. Lin, D. C. Moses, C. H. Hsieh, S. C. Cheng, Y. H. Chen, C. Y. Sun, C. Y. Chou, *Antiviral Res.* **2018**, *150*, 155–163.
- [9] Z. Jin, X. Du, Y. Xu, Y. Deng, M. Liu, Y. Zhao, B. Zhang, X. Li, L. Zhang, C. Peng, Y. Duan, J. Yu, L. Wang, K. Yang, F. Liu, R. Jiang, X. Yang, T. You, X. Liu, X. Yang, F. Bai, H. Liu, X. Liu, L. W. Guddat, W. Xu, G. Xiao, C. Qin, Z. Shi, H. Jiang, Z. Rao, H. Yang, *Nature* **2020**, *582*, 289–293.
- [10] J. He, L. Hu, X. Huang, C. Wang, Z. Zhang, Y. Wang, D. Zhang, W. Ye, *Int. J. Antimicrob. Agents* **2020**, *56*, 106055.
- [11] A. D. Rathnayake, J. Zheng, Y. Kim, K. D. Perera, S. Mackin, D. K. Meyerholz, M. M. Kashipathy, K. P. Battaile, S. Lovell, S. Perlman, W. C. Groutas, K. O. Chang, *Sci. Transl. Med.* **2020**, *12*, eabc5332 (2020).
- [12] V. M. Alves, T. Bobrowski, C. C. Melo-Filho, D. Korn, S. Auerbach, C. Schmitt, E. N. Muratov, A. Tropsha, *Mol. Inf.* **2021**, *40*, 2000113.

- [13] A. K. Ghosh, M. Brindisi, D. Shahabi, M. E. Chapman, A. D. Mesecar, *ChemMedChem* **2020**, *15*, 907–932.
- [14] M. D. Sacco, C. Ma, P. Lagarias, A. Gao, J. A. Townsend, X. Meng, P. Dube, X. Zhang, Y. Hu, N. Kitamura, B. Hurst, B. Tarbet, M. T. Marty, A. Kolocouris, Y. Xiang, Y. Chen, J. Wang, *Sci. Adv.* **2020**, *6*, eabe0751 9.
- [15] J. Qiao, Y.-S. Li, R. Zeng, F.-L. Liu, R.-H. Luo, C. Huang, Y.-F. Wang, J. Zhang, B. Quan, C. Shen, X. Mao, X. Liu, W. Sun, W. Yang, X. Ni, K. Wang, L. Xu, Z.-L. Duan, Q.-C. Zou, H.-L. Zhang, W. Qu, Y.-H.-P. Long, M.-H. Li, R.-C. Yang, X. Liu, J. You, Y. Zhou, R. Yao, W.-P. Li, J.-M. Liu, P. Chen, Y. Liu, G.-F. Lin, X. Yang, J. Zou, L. Li, Y. Hu, G.-W. Lu, W.-M. Li, Y.-Q. Wei, Y.-T. Zheng, J. Lei, S. Yang, *Science* **2021**, eabf1611.
- [16] C. Ma, M. D. Sacco, B. Hurst, J. A. Townsend, Y. Hu, T. Szeto, X. Zhang, B. Tarbet, M. T. Marty, Y. Chen, J. Wang, *Cell Res.* **2020**, *30*, 678–692.
- [17] B. Boras, R. M. Jones, B. J. Anson, D. Arenson, L. Aschenbrenner, M. A. Bakowski, N. Beutler, J. Binder, E. Chen, H. Eng, J. Hammond, R. Hoffman, E. P. Kadar, R. Kania, E. Kimoto, M. G. Kirkpatrick, L. Lanyon, E. K. Lendy, J. R. Lillis, S. A. Luthra, C. Ma, S. Noell, R. S. Obach, M. N. O'Brien, R. O'Connor, K. Ogilvie, D. Owen, M. Pettersson, M. R. Reese, T. Rogers, M. I. Rossulek, J. G. Sathish, C. Steppan, M. Ticehurst, L. W. Updyke, Y. Zhu, J. Wang, A. K. Chatterjee, A. D. Mesecar, A. S. Anderson, C. Allerton, *bioRxiv* **2020**, 1–32.
- [18] Y. Hu, C. Ma, T. Szeto, B. Hurst, B. Tarbet, J. Wang, *ACS Infect. Dis.* **2021**, *7*, 586–597.
- [19] J. A. C. Nascimento Junior, A. M. Santos, L. J. Quintans-Júnior, C. I. B. Walker, L. P. Borges, M. R. Serafini, *Expert Opin. Ther. Pat.* **2020**, *30*, 567–579.
- [20] J. S. Morse, T. Lalonde, S. Xu, W. R. Liu, *ChemBioChem* **2020**, *21*, 730–738.
- [21] G. Das, S. Ghosh, S. Garg, S. Ghosh, A. Jana, R. Samat, N. Mukherjee, R. Roy, S. Ghosh, *RSC Adv.* **2020**, *10*, 28243–28266.
- [22] K. Sargsyan, C. C. Lin, T. Chen, C. Grauffel, Y. P. Chen, W. Z. Yang, H. S. Yuan, C. Lim, *Chem. Sci.* **2020**, *11*, 9904–9909.
- [23] H. Sies, M. J. Parnham, *Free Radical Biol. Med.* **2020**, *156*, 107–112.
- [24] C. Ma, Y. Hu, J. A. Townsend, P. I. Lagarias, M. T. Marty, A. Kolocouris, J. Wang, *ACS Pharmacol. Transl. Sci.* **2020**, *3*, 1265–1277.
- [25] J. Zhang, R. Saad, E. W. Taylor, M. P. Rayman, *Redox Biol.* **2020**, *37*, 101715.
- [26] N. Noguchi, *Arch. Biochem. Biophys.* **2016**, *595*, 109–112.
- [27] J. Kil, E. Lobarinas, C. Spankovich, S. K. Griffiths, P. J. Antonelli, E. D. Lynch, C. G. Le Prell, *Lancet* **2017**, *390*, 969–979.
- [28] S.-H. Sha, J. Schacht, *Expert Opin. Invest. Drugs* **2017**, *26*, 85–96.
- [29] N. Singh, A. C. Halliday, J. M. Thomas, O. Kuznetsova, R. Baldwin, E. C. Y. Woon, P. K. Aley, I. Antoniadou, T. Sharp, S. R. Vasudevan, G. C. Churchill, *Nat. Commun.* **2013**, *4*, 1332–1337.
- [30] C. W. Nogueira, G. Zeni, J. B. T. Rocha, *Chem. Rev.* **2004**, *104*, 6255–6285.
- [31] V. C. Borges, J. B. T. Rocha, C. W. Nogueira, *Toxicology* **2005**, *215*, 191–197.
- [32] N. V. Barbosa, C. W. Nogueira, P. A. Nogara, A. F. De Bem, M. Aschner, J. B. T. Rocha, *Metallomics* **2017**, *9*, 1703–1734.
- [33] R. Zhao, H. Masayasu, A. Holmgren, *Proc. Natl. Acad. Sci. USA* **2002**, *99*, 8579–8584.
- [34] R. Zhao, A. Holmgren, *J. Biol. Chem.* **2002**, *277*, 39456–39462.
- [35] C. Santi, C. Tidei, in *PATAI'S Chem. Funct. Groups*, John Wiley & Sons, Ltd, **2013**, pp. 1–87.
- [36] C. W. Nogueira, J. B. T. Rocha, *Arch. Toxicol.* **2011**, *85*, 1313–1359.
- [37] G. P. Chen, D. M. Ziegler, *Arch. Biochem. Biophys.* **1994**, *312*, 566–572.
- [38] D. M. Ziegler, P. Graf, L. L. Poulsen, W. Stahl, H. Sies, *Chem. Res. Toxicol.* **1992**, *5*, 163–166.
- [39] P. A. Nogara, L. Orian, J. B. T. Rocha, *Comput. Toxicol.* **2020**, *15*, 100127.
- [40] C. A. Menéndez, F. Byléhn, G. R. Perez-Lemus, W. Alvarado, J. J. de Pablo, *Sci. Adv.* **2020**, *6*, eabd0345.
- [41] M. Zmudzinski, W. Rut, K. Olech, J. Granda, M. Giurg, M. Burda-Grabowska, L. Zhang, X. Sun, Z. Lv, D. Nayak, M. Kesik-Brodacka, S. K. Olsen, R. Hilgenfeld, M. Drag, *bioRxiv* **2020**, DOI 10.1101/2020.08.30.273979.
- [42] E. Weglarz-Tomczak, J. M. Tomczak, M. Giurg, M. Burda-Grabowska, S. Brul, *bioRxiv* **2020**, DOI 10.1101/2020.05.20.107052.
- [43] D. Horvath, A. Orlov, D. I. Osolodkin, A. A. Ishmukhametov, G. Marcou, A. Varnek, *Mol. Inf.* **2020**, *39*, 2000080.
- [44] H. Sies, in *Selenium Biol. Med.* (Ed.: W. A.), Springer, Berlin, **1989**, pp. 153–162.
- [45] H. Sies, *Free Radical Biol. Med.* **1993**, *14*, 313–323.
- [46] R. J. Krause, S. C. Glocke, A. R. Sicuri, S. L. Ripp, A. A. Elfarra, *Chem. Res. Toxicol.* **2006**, *19*, 1643–1649.
- [47] T. Schewe, *Gen. Pharmacol.* **1995**, *26*, 1153–1169.
- [48] S. Antony, C. A. Bayse, *Inorg. Chem.* **2011**, *50*, 12075–12084.
- [49] J. Zhang, E. W. Taylor, K. Bennett, R. Saad, M. P. Rayman, *Am. J. Clin. Nutr.* **2020**, *111*, 1297–1303.
- [50] A. Moghaddam, R. A. Heller, Q. Sun, J. Seelig, A. Cherkezev, L. Seibert, J. Hackler, P. Seemann, J. Diegmann, M. Pilz, M. Bachmann, W. B. Minich, L. Schomburg, *Nutrients* **2020**, *12*, 2098.
- [51] L. Wang, Z. Yang, J. Fu, H. Yin, K. Xiong, Q. Tan, H. Jin, J. Li, T. Wang, W. Tang, J. Yin, G. Cai, M. Liu, S. Kehr, K. Becker, H. Zeng, *Free Radical Biol. Med.* **2012**, *52*, 898–908.
- [52] S. Hariharan, S. Dharmaraj, *Inflammopharmacology* **2020**, *28*, 667–695.
- [53] C. W. Nogueira, J. B. T. Rocha, *J. Braz. Chem. Soc.* **2010**, *21*, 2055–2071.
- [54] A. S. Weisberger, L. G. Suhrlund, *Blood* **1956**, *11*, 19–30.
- [55] O. Trott, A. J. Olson, *J. Comput. Chem.* **2010**, *31*, 455–461.
- [56] E. F. Pettersen, T. D. Goddard, C. C. Huang, G. S. Couch, D. M. Greenblatt, E. C. Meng, T. E. Ferrin, *J. Comput. Chem.* **2004**, *25*, 1605–1612.
- [57] J. Osipiuk, C. Tesar, M. Endres, V. Lisnyak, S. Maki, C. Taylor, Y. Zhang, Z. Zhou, S. A. Azizi, K. Jones, R. Kathayat, S. A. Snyder, B. C. Dickinson, A. Joachimiak, “The crystal structure of Papain-Like Protease of SARS CoV-2 in complex with PLP_Snyder441,” DOI 10.2210/pdb7JN2/pdb, **2020**.
- [58] M. D. Hanwell, D. E. Curtis, D. C. Lonie, T. Vandermeersch, E. Zurek, G. R. Hutchison, *J. Cheminf.* **2012**, *4*, 1–17.
- [59] J. J. P. Stewart, MOPAC 2016 program, Colorado Springs, CO (USA), **2016**.
- [60] J. J. P. Stewart, *J. Mol. Model.* **2007**, *13*, 1173–1213.
- [61] A. Müller, H. Gabriel, H. Sies, *Biochem. Pharmacol.* **1984**, *33*, 3241–3245.
- [62] G. Bianco, S. Forli, D. S. Goodsell, A. J. Olson, *Protein Sci.* **2016**, *25*, 295–301.
- [63] M. A. T. van de Plassche, M. Barniol-Xicota, S. H. L. Verhelst, *ChemBioChem* **2020**, *21*, 3383–3388.
- [64] F. Neese, *WIREs Comput. Mol. Sci.* **2012**, *2*, 73–78.
- [65] F. Neese, *WIREs Comput. Mol. Sci.* **2018**, *8*, e1327.
- [66] M. Swart, A. W. Ehlers, K. Lammertsma, *Mol. Phys.* **2004**, *102*, 2467–2474.
- [67] E. Van Lenthe, E. J. Baerends, J. G. Snijders, *J. Chem. Phys.* **1994**, *101*, 9783–9792.

- [68] F. Zaccaria, L. P. Wolters, C. Fonseca Guerra, L. Orian, *J. Comput. Chem.* **2016**, *37*, 1672–1680.
- [69] G. Ribaudo, M. Bellanda, I. Menegazzo, L. P. Wolters, M. Bortoli, G. Ferrer-Sueta, G. Zagotto, L. Orian, *Chem. A Eur. J.* **2017**, *23*, 2405–2422.
- [70] M. Bortoli, M. D. Tiezza, C. Muraro, G. Saielli, L. Orian, *Molecules* **2019**, *24*, 1250.
- [71] A. Madabeni, M. Dalla Tiezza, F. B. Omege, P. A. Nogara, M. Bortoli, J. B. T. Rocha, L. Orian, *J. Comput. Chem.* **2020**, *41*, 2045–2054.
- [72] H. Jónsson, G. Mills, K. W. Jacobsen, in *Class. Quantum Dyn. Condens. Phase Simulations* (Eds.: B. J. Berne, G. Ciccotti, D. F. Coker), World Scientific, Singapore, **1998**, pp. 385–404.
- [73] W. Dai, B. Zhang, X.-M. Jiang, H. Su, J. Li, Y. Zhao, X. Xie, Z. Jin, J. Peng, F. Liu, C. Li, Y. Li, F. Bai, H. Wang, X. Cheng, X. Cen, S. Hu, X. Yang, J. Wang, X. Liu, G. Xiao, H. Jiang, Z. Rao, L.-K. Zhang, Y. Xu, H. Yang, H. Liu, *Science* **2020**, *368*, 1331–1335.
- [74] N. Lobo-Galo, M. Terrazas-López, A. Martínez-Martínez, Á. G. Díaz-Sánchez, *J. Biomol. Struct. Dyn.* **2020**, *1*, 1–9.
- [75] A. B. Gurung, M. A. Ali, J. Lee, M. Abul Farah, K. M. Al-Anazi, *Saudi J. Biol. Sci.* **2020**, *27*, 2674–2682.
- [76] R. Jain, S. Mujwar, *Struct. Chem.* **2020**, *31*, 2487–2499.
- [77] A. T. Ton, F. Gentile, M. Hsing, F. Ban, A. Cherkasov, *Mol. Inf.* **2020**, *39*, 2000028.
- [78] S. V. Stoddard, S. D. Stoddard, B. K. Oelkers, K. Fitts, K. Whalum, K. Whalum, A. D. Hemphill, J. Manikonda, L. M. Martinez, E. G. Riley, C. M. Roof, N. Sarwar, D. M. Thomas, E. Ulmer, F. E. Wallace, P. Pandey, S. Roy, *Viruses* **2020**, *12*, 942.
- [79] R. Yoshino, N. Yasuo, M. Sekijima, *Sci. Rep.* **2020**, *10*, 12493.
- [80] Y. M. Báez-Santos, S. E. St. John, A. D. Mesecar, *Antiviral Res.* **2015**, *115*, 21–38.
- [81] W. Rut, Z. Lv, M. Zmudzinski, S. Patchett, D. Nayak, S. J. Snipas, F. El Oualid, T. T. Huang, M. Bekes, M. Drag, S. K. Olsen, *Sci. Adv.* **2020**, *6*, eabd4596.
- [82] S. Ullrich, C. Nitsche, *Bioorg. Med. Chem. Lett.* **2020**, *30*, 127377.
- [83] J. T. Ortega, M. L. Serrano, B. Jastrzebska, *Biomol. Eng.* **2020**, *10*, 1–19.
- [84] S. Skariyachan, D. Gopal, S. Chakrabarti, P. Kempanna, A. Uttarkar, A. G. Muddebhalkar, V. Niranjana, *Comput. Biol. Med.* **2020**, *126*, 104054.
- [85] M. Cassandri, A. Smirnov, F. Novelli, C. Pitolli, M. Agostini, M. Malewicz, G. Melino, G. Raschellà, *Cell Death Dis.* **2017**, *3*, 17071.
- [86] C. Abbehausen, *Metallomics* **2019**, *11*, 15–28.
- [87] A. M. Rydzik, J. Brem, W. B. Struwe, G. T. Kochan, J. L. P. Benesch, C. J. Schofield, *Bioorg. Med. Chem. Lett.* **2014**, *24*, 4954–4957.
- [88] I. K. H. Leung, T. J. Krojer, G. T. Kochan, L. Henry, F. von Delft, T. D. W. Claridge, U. Oppermann, M. A. McDonough, C. J. Schofield, *Chem. Biol.* **2010**, *17*, 1316–1324.
- [89] D. E. K. Sutherland, M. J. Stillman, *Metallomics* **2011**, *3*, 444–463.
- [90] A. Ziller, L. Fraissinet-Tachet, *Metallomics* **2018**, *10*, 1549–1559.
- [91] N. Mills-Davies, D. Butler, E. Norton, D. Thompson, M. Sarwar, J. Guo, R. Gill, N. Azim, A. Coker, S. P. Wood, P. T. Erskine, L. Coates, J. B. Cooper, N. Rashid, M. Akhtar, P. M. Shoolingin-Jordan, *Acta Crystallogr. Sect. D* **2016**, *73*, 9–21.
- [92] E. K. Jaffe, *Acc. Chem. Res.* **2016**, *49*, 2509–2517.
- [93] C. Jacob, W. Maret, B. L. Vallee, *Biochem. Biophys. Res. Commun.* **1998**, *248*, 569–573.
- [94] J. B. T. Rocha, R. A. Saraiva, S. C. Garcia, F. S. Gravina, C. W. Nogueira, *Toxicol. Res. (Camb)* **2012**, *1*, 85–102.
- [95] P. A. Nogara, J. B. T. Rocha, *Mol. Inf.* **2018**, *37*, 1700091.
- [96] P. B. Lutz, C. A. Bayse, *J. Inorg. Biochem.* **2016**, *157*, 94–103.
- [97] G. Andrés Cisneros, W. Yang, in *Challenges Adv. Comput. Chem. Phys.* (Eds.: Y. D. M., L. T. S.), Springer, Dordrecht, **2009**, pp. 57–78.
- [98] R. Kirikoshi, N. Manabe, O. Takahashi, *Int. J. Mol. Sci.* **2018**, *19*, 637.
- [99] J. Liu, Y. Zhang, C.-G. Zhan, *J. Phys. Chem. B* **2009**, *113*, 16226–16236.
- [100] T. Nakayoshi, K. Kato, S. Fukuyoshi, O. Takahashi, E. Kurimoto, A. Oda, *Biochim. Biophys. Acta Proteins Proteomics* **2018**, *1866*, 759–766.
- [101] V. Ullrich, P. Weber, F. Meisch, F. Von Appen, *Biochem. Pharmacol.* **1996**, *52*, 15–19.
- [102] G. Wagner, G. Schuch, T. P. M. Akerboom, H. Sies, *Biochem. Pharmacol.* **1994**, *48*, 1137–1144.
- [103] G. K. Azad, R. S. Tomar, *Mol. Biol. Rep.* **2014**, *41*, 4865–4879.
- [104] D. Steinmann, T. Nauser, W. H. Koppenol, *J. Org. Chem.* **2010**, *75*, 6696–6699.
- [105] B. K. Sarma, G. Mugesh, *J. Am. Chem. Soc.* **2005**, *127*, 11477–11485.
- [106] J. He, D. Li, K. Xiong, Y. Ge, H. Jin, G. Zhang, M. Hong, Y. Tian, J. Yin, H. Zeng, *Bioorg. Med. Chem.* **2012**, *20*, 3816–3827.
- [107] V. Nascimento, P. S. Cordeiro, M. Arca, F. Marini, L. Sancineto, A. L. Braga, V. Lippolis, M. Iwaoka, C. Santi, *New J. Chem.* **2020**, *44*, 9444–9451.
- [108] M. Pietka-Ottlik, P. Potaczek, E. Piasecki, J. Mlochowski, *Molecules* **2010**, *15*, 8214–8228.
- [109] B. K. Sarma, G. Mugesh, *Chem. Eur. J.* **2008**, *14*, 10603–10614.
- [110] C. Lambert, R. Cantineau, L. Christiaens, J. Biedermann, N. Dereu, *Bull. des Sociétés Chim. Belges* **1987**, *96*, 383–389.
- [111] S. Kumar, H. B. Singh, G. Wolmershäuser, *Organometallics* **2006**, *25*, 382–393.
- [112] L.-Y. Sun, C. Chen, J. Su, J.-Q. Li, Z. Jiang, H. Gao, J.-Z. Chigan, H.-H. Ding, L. Zhai, K.-W. Yang, *Bioorg. Chem.* **2021**, *112*, 104889.

Received: April 7, 2021

Accepted: April 11, 2021

Published online on May 21, 2021